EVOLUTION OF VOIDS DURING DUCTILE CRACK PROPAGATION IN AN AL ALLOY SHEET TOUGHNESS TEST STUDIED BY SYNCHROTRON RADIATION COMPUTED TOMOGRAPHY

T.F. Morgeneyer[1,2,a], M.J. Starink[1,b] and I.Sinclair[1,c]

[1]Materials Research Group, School of Engineering Sciences, University of Southampton, Southampton, SO17 1BJ, United Kingdom

[2] Alcan Centre de Recherches de Voreppe, BP 27, 38341 Voreppe Cedex, France

[a] tm504@soton.ac.uk, [b] m.j.starink@soton.ac.uk, [c] i.sinclair@soton.ac.uk

Abstract

The anisotropy of fracture toughness in AA2139 (Al-Cu-Mg) alloy sheet has been investigated via synchrotron radiation computed tomography of arrested cracks in Kahn tear test pieces for different loading cases. The three dimensional distribution and morphology of pores and defects in the as-received state are seen to be anisotropic, with chains of voids and void elongation in the L (longitudinal) direction. For toughness testing in L-T orientation (T is long transverse), voids ahead of the crack grow and link in the L direction. In T-L tests, voids ahead of the crack tip also grow in the loading direction, although a high degree of alignment is retained in the L direction. The present work provides quantitative microstructural data that can be used as input for and validation of recent idealised model formulations, and it is shown that the measured void dimensions and evolution are consistent with measured toughness anisotropy.

1.   Introduction

Fracture toughness is a crucial material design criterion for many high strength materials applications [1,2]. Historically, two dimensional (2D) surface imaging techniques, such as optical and electron microscopy, have been used to reveal fracture micromechanisms [3,4]. With recent developments in synchrotron radiation computed tomography (SRCT) it has become possible to visualise fracture mechanisms within materials at a sub-micron scale in three dimensions (3D) [5]. Classical treatments of ductile crack growth have highlighted the geometrical aspects of damage evolution, particularly in relation to the later stages of void coalescence. The work of Hahn and Rosenfield [6] for example simply identifies the critical condition for fracture toughness with inter-void separation distance and degree of crack tip opening ('void-by-void' growth [7]). More recent works [8-13] have recognised the inevitable complications of failure in 'real'

engineering materials, where defect/void distributions associated with fracture are often subject to complex patterns of spatial clustering and/or anisotropy, along with wide/multi-modal distributions in size and morphology. To date, even the most complex contemporary treatments of ductile failure [7-13] involve a variety of microstructural and micromechanical simplifications. In this respect, detailed 3D micromechanical observations of fracture/damage evolution in real microstructures may provide an important basis for parametric initialisation and validation of such models.

The present study focuses on tomographic observation of fracture in an Al-Cu-Mg alloy sheet. The primary application is for airframe manufacture, where toughness and fatigue resistance are critical. With recent progress in SRCT, several studies on the micromechanisms of failure in Al alloys have been reported.   Using *in-situ* tests Qian *et al.* [14] highlight the growth of voids and their coalescence during ductile fracture of a notched specimen geometry via SRCT. Fatigue crack closure phenomena have also been observed and quantified by various researchers [15-18].

Maire *et al.* [19] have quantitatively assessed the monotonic growth of voids in a model aluminium matrix composite containing spherical ceramic particles; through careful matching of experimental

conditions and parallel model formulation (*e.g.* in terms of damage volume fraction and triaxiality levels), good accord was obtained between experimental and predicted void growth behaviour.

The present work reports on the novel SRCT observation of ductile crack extension in an anisotropic high strength Al-alloy sheet, going from parent (unstrained) material to the point of coalescence with a propagating crack tip, via the analysis of arrested crack growth specimens. In particular, the relationship between prior defect geometry, spatial distribution and the micromechanisms of failure have been observed for two test orientations.

2.   Experimental

AA2139 sheet was supplied by Alcan CRV with a thickness of 3.2mm. The nominal composition is given in Table 1. After solution treatment, the plate was stretched by 2%, then aged at 175 °C for 16 hours. The tensile properties of the material such as tensile yield strength (TYS) and ultimate tensile strength (UTS) are given in Table 2. The plastic anisotropy of the material is very small.

The grain size was obtained from optical microscopy on etched sections using a mean linear intercept method as 60 μm in rolling direction (L), 52 in long transverse direction (T) and 24 μm in short-transverse direction (S).

A field emission gun scanning electron microscope (JEOL 6500F) equipped with an electron dispersive spectroscopy (EDS) analyser was used to assess material microstructures. EDS analysis revealed two populations of intermetallic particles: $Al_7Cu_2(Fe,Mn)$ and Al_2Cu. The particles were strongly aligned as stringers in the rolling direction (L) with stringer dimensions of the order of 15-30μm (*cf.* 1-10μm in the long transverse direction (T) and 1-6μm in the short-transverse direction (S)). The intermetallic content has been measured via grey value thresholding of field emission gun scanning electon microscope (FEG-SEM) images (backscattered electron mode) to be ~0.004 ±15% (standard error based on repeat measurements at different magnifications).

Cracks were grown to a length of 10mm in Kahn tear test [20] pieces (dimensions: 35mm x 60mm x 3.2mm) in general accord with ASTM B 871 - 01: *i.e.* tests were arrested before final failure of the coupon. At 10mm from the notch the crack is slanted. To facilitate high resolution SRCT imaging

of the arrested crack tip region, a small 'stick' of material (dimensions 1mm x 1mm x 10mm) was extracted around the tip at the specimen mid-plane (long dimension parallel to the direction of crack extension) using a slow speed diamond saw, see Figure 1.

Mechanical testing and subsequent SRCT crack tip imaging has been performed in both the L-T and T-L configurations, *i.e.* in-plane testing, with loading applied in the rolling and long transverse directions respectively, see Figure 2. Unit initiation energies (UIE) have been calculated using the crosshead displacement and accounting for machine stiffness. The UIE value for T-L loading is ~ 79N/mm and for L-T loading ~104N/mm .

 Tomography was performed at beamline ID 19 of the European Synchrotron Radiation Facility (ESRF), Grenoble, France, at 20.5kV. The facility provides a highly coherent, spacially and spectrally homogeneous beam with a high photon flux. For one volume 1500 radiographs were taken using a high performance CCD camera whilst the sample was turned through 180° (parallel beam conditions) in steps of 0.12°; the typical imaging time per radiograph was 0.7s. Flat-field and dark current corrections were performed and reconstruction was carried out using a conventional filtered back projection algorithm [5]. In the reconstructed slices an isotropic voxel size of 0.7μm was obtained. Phase contrast imaging has been performed to enhance the detection of edges [21]. At ID19 this is a straightforward technique as advantage is taken of the radiation coherence by adjusting the sample-detector distance (13mm in the present work) to obtain near-field Fresnel diffraction effects. Detailed information on the imaging techniques is given in [22].

Subsequent 2D and 3D imaging and analysis was carried out using the commercial software package 'VG Studio Max v1.2' [23]. Use was made of a "sum along ray" visualisation [24]. Specifically, the imaged volumes containing the crack tip and associated microstructural features have been segmented (in 3D) and shown in isolation from the surrounding aluminium matrix. A 'box-car' transformation is used to fill the crack/defects with voxels of equal grayscale, which are then viewed perpendicular to the nominal crack plane. The "sum along ray" method (see Figure 3) then generates a projection of the crack plane, where the grey level is directly proportional to the crack thickness, *i.e.* a crack opening displacement (COD) map is obtained.

SRCT measurements of the prior pore content of the material (i.e. before loading) were carried out (sampling volume of 980μm x 490μm x 490μm). For the arrested cracks, the evolution of damage/voids ahead of the growing crack tip has been characterised in a similar sampling volume at a distance of some 70μm ahead of the overall crack tip location (representing a region of reasonably uniform damage evolution, ahead of local fluctuations in the main crack tip location and coalescence).

3.   Results

3.1. Kahn tear test results

Figure 4 shows the results of Kahn tear tests in terms of force divided by the initial ligament area A_0 as a function of the crack mouth opening displacement (CMOD) and the crack length as a function of the CMOD. It can be seen that the T-L sample is less tough than the L-T sample, as for the T-L sample the nominal stress in the propagation region is lower and the crack growth is faster than for the L-T sample (particularly up to ~15mm of crack extension). Average unit initiation energies were measured to be ~30% higher in the L-T orientation compared to the T-L.

.

3.2. SRCT of the as-received material

Figure 5 shows typical 2D sections from the SRCT data taken in the as received, undeformed material. The aluminium matrix (grey), intermetallics (white) and pores (black) are clearly delineated, with phase contrast fringes highlighting the associated edges/interfaces. Pore content determination variation of the non-deformed material was governed by the choice of the grey scale threshold. Pore content is expected to be 0.0034 with a variation of ±10% when setting extreme grey values. Mean pore dimensions (3D Feret measurements) are 7.6, 5.4 and 4.5 μm in the L, T and S directions respectively. 3D Voronoi tessellation [25] of the void distribution revealed average cell dimensions of 45 and 48μm in the L and T direction respectively, i.e. indicative of near-

neighbour separation distances in these directions. Pores were seen to be closely linked with the intermetallic distribution, with a large proportion being associated with one or more intermetallic particles. The alignment of pores into local chains in the L-direction is also evident in Figure 5(a).

Figure 6 further shows a 3D rendering of the void distribution of the as received material (*i.e.* with the aluminium matrix and secondary phase particles being rendered transparent). It should be noted that the intrinsic void content of the parent material is of course 'exaggerated' by the 3D nature of Figure 6, representing the void content of a thick slice of material (350μm x 350μm x 180μm) rather than a 2D section in traditional metallographic imaging. The more marked elongation in the L direction is again evident, with mean 3D Feret dimension aspect ratios of every pore in Fig. 6 (i.e. for whole pores, as opposed to section planes) being measured as ~ 1.6, 1.2 and 1.5 in the L-S, T-S and L-T planes respectively.

3.3. SRCT of the arrested cracks

Figure 7 shows 2D sections of the material undergoing slant fracture at the crack tip. In Figure 7(a) results for the L-T test orientation are shown, i.e. corresponding to crack growth in the T direction, with elongated voids being discernable in the loading direction, L. Figure 7(b) shows the T-L case, where voids are again elongated in the loading direction (the T direction in this case) but to a lesser extent than in Figure 7(a). In conjunction with SEM fracture surface assessment, the crack itself is seen to be made up of both coarse voids (of the order of 20μm diameter) and regions of shear decohesion. Coarse voids arise from both intermetallic particle cracking and decohesion, although with the prior presence of pores in the parent material and the observed correlation of intrinsic pores with intermetallics it is clearly difficult to discern the exact origin of each crack tip void (i.e. distinguishing growth of pores that where already present from intermetallic decohesion). It is discernable from Figure 7 however that a significant proportion of the intermetallics (particularly smaller ones) do not exhibit pores in the immediate vicinity of the crack.

Figure 8 and 9 show 3D images of the distribution of voids immediately ahead of the crack tip (~50μm ahead of the main crack tip). Similar to Figure 6 the Al matrix is transparent in this case and only the voids can be seen. The elongation of voids in the loading direction is particularly apparent in Figure 8(a); void aspect ratios for loading in rolling direction (L) are clearly higher than those for the T-direction loading (Figure 8(b)): the mean Feret dimension aspect ratio of every void for the L-T load cases in the L-S plane is ~2.0 and for the T-L load cases in the T-S plane it is ~1.6, whilst in the L-T plane the mean Feret dimension aspect ratios for the L-T and T-L load cases are ~1.6 and ~1.1 respectively. A number of extremely elongated voids are seen in the L-T load case (see Figure 10), with the morphology of these implying that just ahead of the crack tip pore chains which existed in the L direction prior to testing have coalesced into highly elongated single bodies ("void columns"). Such behaviour has been noted in theoretical models [13], however the present results may be identified with a plane stress state (low lateral stresses) as compared to the high lateral stress condition considered in [13].

Figure 11 shows a comparison of the crack tip regions for the L-T and T-L loading cases distinguishable from narrower shear coalescence regions as the thick regions appear brighter than the thin ones. Comparison of void position in Figure 11(a) and (b) shows that in the region of coalescence at the crack tip the spacing between large/primary voids is larger for the L-T testing case (the tougher direction). This is further reflected in the number density of voids in this region in the L-T sample, measured as ~230/mm^2, whilst for the T-L sample it was approximately 20% higher (~270/mm^2). Coalesced void chains are also evident in the crack growth direction in the T-L case, see Figure 11(b). In this figure one void chain is magnified, and several other brighter chains are also evident (see dashed boxes indicating examples of void chains). It may be seen that at the crack front such chains extend some 50-100μm ahead of the surrounding crack front location: such local extensions of the crack are not seen in the tougher, L-T oriented test. In the L-T loading case the coalescing voids in the L direction have a final strongly elongated form (aspect ratios of up to ~ 4), *cf.* the T direction loading where an essentially penny-shaped void morphology is attained

immediately before crack coalescence (void shape extended in the loading and crack growth direction). On the fracture surface for the L-T loading case the average apparent void length in the crack growth direction (T in this case) is 35μm whilst for the T-L loading case the average apparent void length on the fracture surface in the crack direction (L in this case) is 45μm.

4. Discussion

From the tomography observations, the sequence of events during fracture of the present Al-Cu-Mg alloy sheet may be discerned as follows: initially the material displays a classically anisotropic intermetallic and pore distribution for a rolled material, both appearing as aligned chains elongated in the rolling direction (L). Subsequent loading in the L direction leads to the coalescence of chains of voids in the loading direction so that large voids that are highly elongated in the rolling direction are created prior to coalescence at the crack tip (see figure 8), i.e. coalescence occurs heterogeneously and is a multi-stage process. Concerning the T-L case, voids are seen to grow in the loading direction, but remain primarily elongated in the rolling direction, reflecting the prior pore distribution of the parent material. Inter-void separation distances at coalescence are reduced *cf.* the L-T case, and the incidence of void coalescence in chains is seen parallel to the growth direction just ahead of the crack tip.

In the present analysis it is useful to recall the model by Tvergaard and Hutchinson [7] which provides a formulation and numerical analysis of a two-dimensional plane strain model with multiple discrete voids located ahead of a pre-existing crack tip. At initial void volume fractions that are sufficiently low, initiation and growth is approximately represented by the void by void mechanism [7]. At somewhat higher initial void volume fractions, a transition in behavior occurs whereby many voids ahead of the tip grow at comparable rates and their interaction determines initiation toughness and crack growth resistance [7]. For intermediate void volume fractions a 'hybrid' condition of void-by-void and multiple void coalescence may be encountered. Given the heterogeneous distribution of prior pores/intermetallics in our material, the void coalescence observed in the T-L case may be identified with this 'hybrid' condition. Detailed comparison of

current void distributions and Tvergaard and Hutchinson's [7] prediction are difficult (contingent on various modelling parameters and assumptions), however, it may be seen that a consequence of Tvergaard and Hutchinson's [7] prediction of prior void volume fractions for void coalescence mode transitions falling close to the effective initial void content of the present material does imply that a hybrid failure mode may easily arise when voids are heterogeneously dispersed and significant local fluctuations in volume fraction are produced.

Given the elongated prior pore and intermetallic content of the present sheet material, fracture modelling results for prolate and oblate initial void shapes, as described in Refs. [8-11], are of some interest, although the present voids do not exactly present such axisymmetric morphologies. In the work of Pardoen and Hutchinson [10], toughness effects of pore shape and spatial alignment are presented [10], at least for regular (non-clustered) distributions of pores, with predictions being made in terms of plane strain J_{IC} values. The Finite Element analysis of Pardoen and Hutchinson [10] has been carried out considering plane strain, small scale yielding conditions and only one value for the strain hardening exponent (n=0.1). Following from the known correlation of UIE and K_{IC} values [26], it is possible to at least compare the magnitude of predicted and experimental changes in toughness value with test orientation. Interpolation of results provided by Pardoen and Hutchinson [10] show that for uniformly dispersed prolate and oblate voids of aspect ratio 1.5 and 0.67 respectively at an initial pore fraction in the order of 0.5 to 0.8%, i.e. aspect ratios equivalent to those presented by the L-T and T-L tests and volume fraction of the order of the initial defect content of the alloy (pores plus intermetallics), J_{IC} should decrease by 20-30% between L-T and T-L tests. As such, the shapes of voids and volume fraction of defects are reasonably consistent with the measured difference in UIE between L-T and T-L Kahn tests of our alloy, which was about 30%. Pardoen and Hutchinson [10] further consider the influence of directional alignment of spherical voids on toughness, as illustrated in Figure 12, it is difficult to identify appropriate values for the regular spacings X_0^A and X_0^B in the model from the real 3D microstructure, which has substantial statistical variations.

However, their ratio may in the first instance be anticipated to scale with the aspect ratio of Voronoi cells generated for the microstructure in the L-T plane. From tessellation analysis on the tomography data of as received samples we obtained a value of ~1.0 for the ratio of 3D Feret dimensions in L and T of the Voronoi cells, suggesting that the pore spacing may not be a primary contribution to fracture anisotropy. Thus the present analyses suggest that it is the shape of the voids rather than their distribution that causes the difference in toughness between the two orientation. It should be noted however that comparison of experimental and modelled toughness values are subject to many simplifications in this instance (*e.g.* simplified void shapes, spatial arrangement, matrix work hardening and plastic isotropy), and the significance of average pore spacing parameters when alignment occurs within local clusters is not known.

5. Conclusions

- Kahn tear test on an Al-Cu-Mg sheet has shown toughness anisotropy: T-L samples are less tough than L-T samples.

- The evolution of voiding/damage during ductile crack growth has been observed via high resolution tomography in a high strength Al-alloy, showing the evolution of void growth and coalescence processes.

- The undeformed, as-received material has been investigated showing anisotropic distribution of pores: elongated aligned pores are prevalent in rolling direction

- In the case of loading in L direction (crack growth in T) voids ahead of the crack may link in the loading direction (L) and form large strongly prolate voids prior to crack coalescence

- In the case of loading in the T direction (crack growth in L), voids ahead of the crack tip have grown in the loading direction (T) but retain significant elongation in the L direction, i.e. are close to penny-shaped as coalescence occurs.

- The "sum along ray" representation of the crack in both samples elucidates that separation distances between coarse voids are shorter for crack growth in L direction than for crack growth in T direction , consistent with the measured toughness anisotropy.

- Toughness trends are in semi-quantitative accord with recent local approach finite element models of idealised void shape, distribution and alignment effects, notwithstanding the simplifications required to make these comparisons.

Acknowledgements

References

[1] Cho A, Bes B. Mater Sci Forum 2006 ; 519-521 : 603-608

[2] Warner T. Mater Sci Forum 2006 ; 519-521 : 1271-1278

[3] Haynes MJ, Gangloff RP. Metall Mater Trans A 1998; 29A, 1599-1613

[4] Ludtka GM, Laughlin DE. Metall Trans A 1982; 13A, 411-425

[5] Maire E, Buffière J-Y, Salvo L, Blandin JJ, Ludwig W, Letang J M. Adv Eng Mat 2001; 3:539-546

[6] Hahn GT, Rosenfield AR. Metall Trans A 1975;6A:653-668

[7] Tvergaard V, Hutchinson J H. Int J Solids Struct 2002;39:3581-3597

[8] Gologanu M, Leblond JB, Devaux J. J Mech Phys Solids 1993;41:1723-1784

[9] Gologanu M, Leblond JB, Devaux J. Trans ASME, J Eng Mater Technol 1994;116:290-297

[10] Pardoen T, Hutchinson JW. Acta Met 2003;51:133-148

[11] Lassance D, Scheyvaerts F, Pardoen T. Eng Fract Mech 2006;73:1009-1034

[12] Decamp K, Bauvineau L, Besson J, Pineau A. Int J Fract 1997 ;88 :1-18

[13] Gologanu M, Leblond JB, Devaux J. Int J Solids Struct 2001;38:5595-5604

[14] Qian L, Toda H, Uesugi K, *et al.* Appl Phys Lett 2005;87:241907-241910

[15] Khor KH, Buffière J-Y, Ludwig W, *et al.* J Phys Condens Matter 2004;16:3511-3515

[16] Toda H, Sinclair I, Buffière J-Y, *et al.* Acta Mat 2004 ;52 :1305-1317

[17] Guvenilir A, Stock S R, Fatigue Fract Eng Mater Struct 1998;21:439-450

[18] Guvenilir A, Breunig, T M, Kinney J H, Stock S R. Acta Mater 1997;45:1977-1987

[19] Maire E, Bordreuil C, Babout L, *et al.* J. Mech Phys Solids 2005;53:2411-2434

[20] ASTM-international, Standard B 871 - 01. 2001.

[21] Kocsis M, Snirgirev A. Nucl Instrum Methods Phys Res Sect A 2004;525A:79-84

[22] Ludwig W. *Development and Applications of Synchrotron Radiation Microtomography*, Dissertation der LMU München, München, 2001

[23] VGStudio Max 1.2, Volume Graphics GmbH

[24] Toda H, Sinclair I, Buffière J-Y *et al*. Philos Mag 2003;83:2429-2440

[25] Yang N., Boselli J., Sinclair, I. J Microsc 2001;201: 189-200

[26] Dumont D, Deschamps A, Brechet Y. Mat Sci Eng A 2003;A356:326-336

Tables

Table 1

alloy	Si	Fe	Cu	Mn	Mg	Ag	Ti	Zn
2139	<= 0.1	<= 0.15	4.5 - 5.5	0.20 - 0.6	0.20 - 0.8	0.15 - 0.6	<= 0.15	<=0.25

Table 1 Composition limits of alloy AA2139 in weight %

direction	L	T
TYS in MPa	440	430
UTS in MPa	478	475

Table 2: Tensile properties of alloy AA2139 in T8 condition for testing directions L and T

Figures

Figure 1
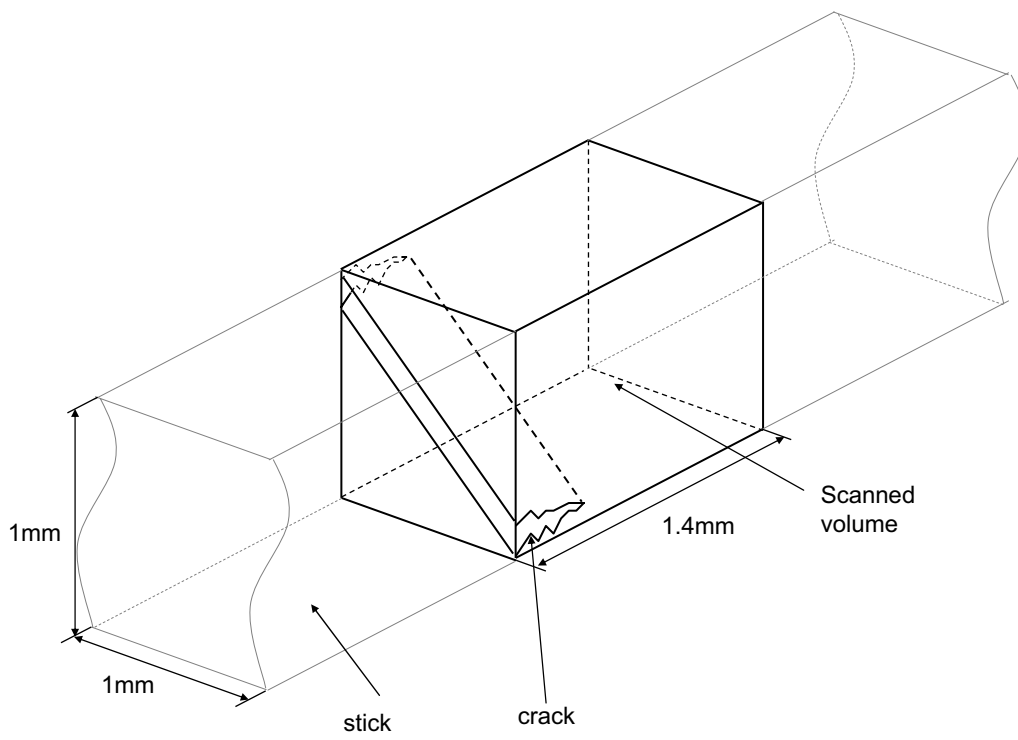
Figure 1: Schematic drawing of the investigated volume at the arrested crack tips.

Figure 2
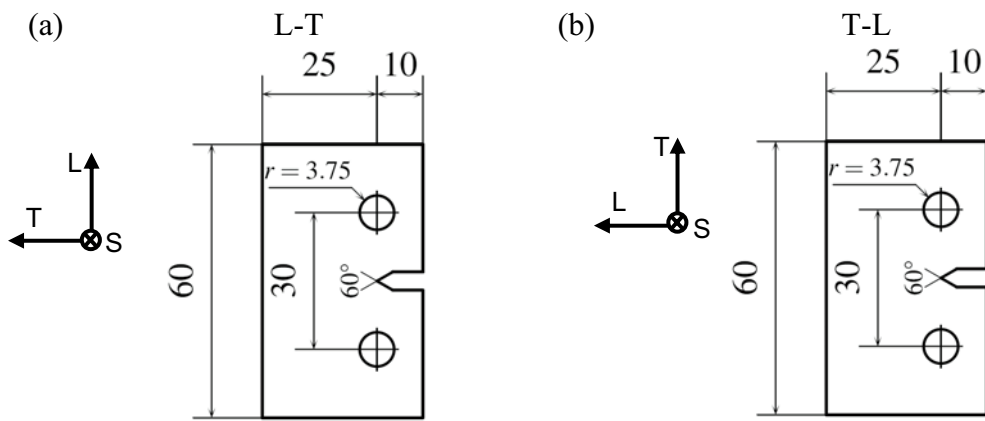
Figure 2: Sample and loading geometries: (a) L-T and (b) T-L; all dimensions in mm

Figure 3
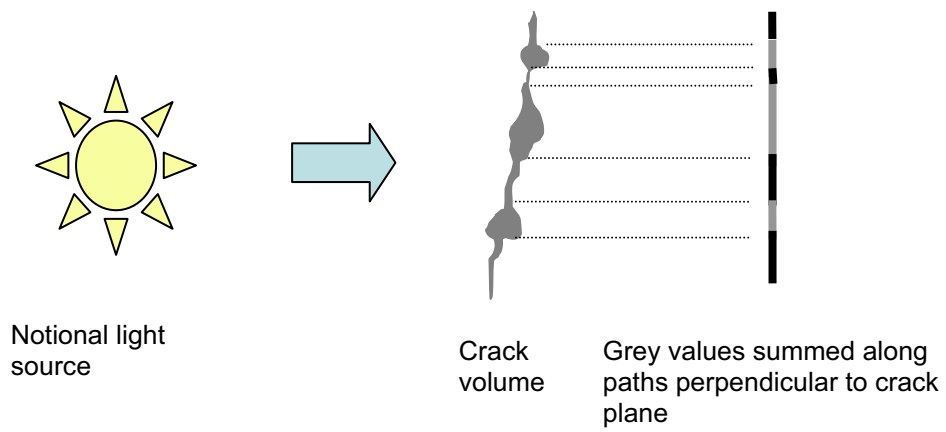
Figure 3: Schematic 2D illustration of the "sum along ray" algorithm: in the final projection of the

crack thicker areas, in this instance associated with void growth, appear bright/white.

Figure 4
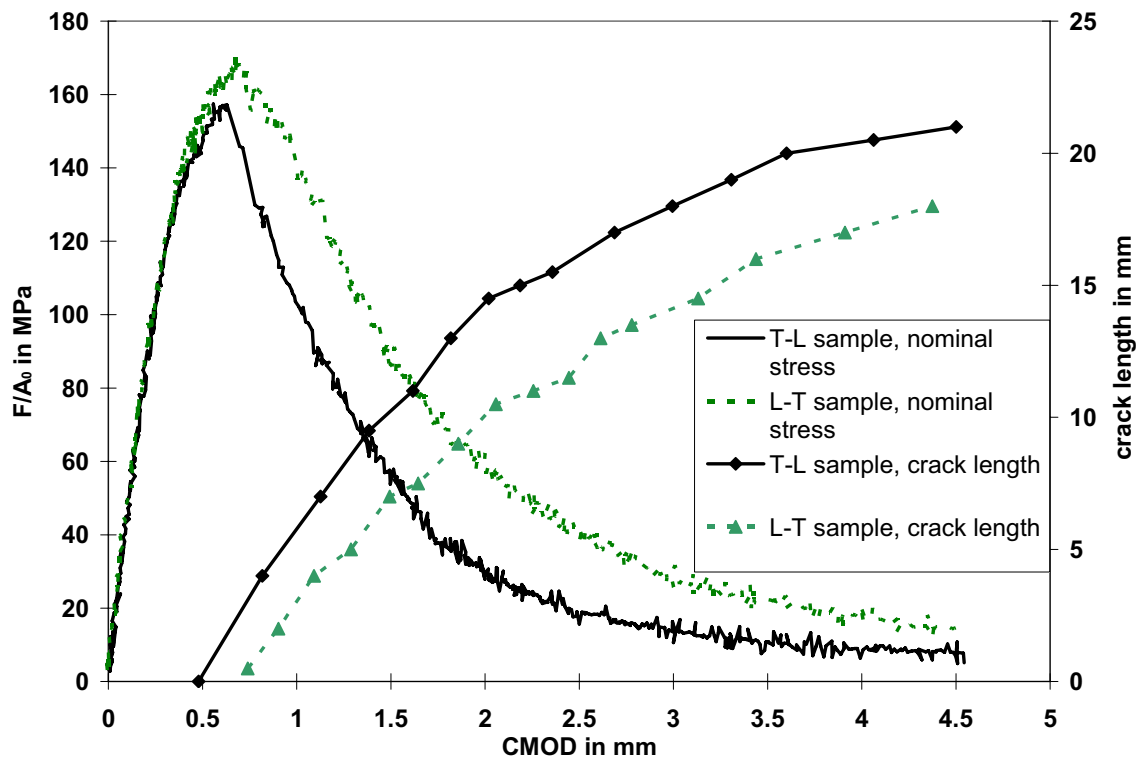
Figure 4: Results of the Kahn tear tests for the T-L and L-T samples.

Figure 5

(a)
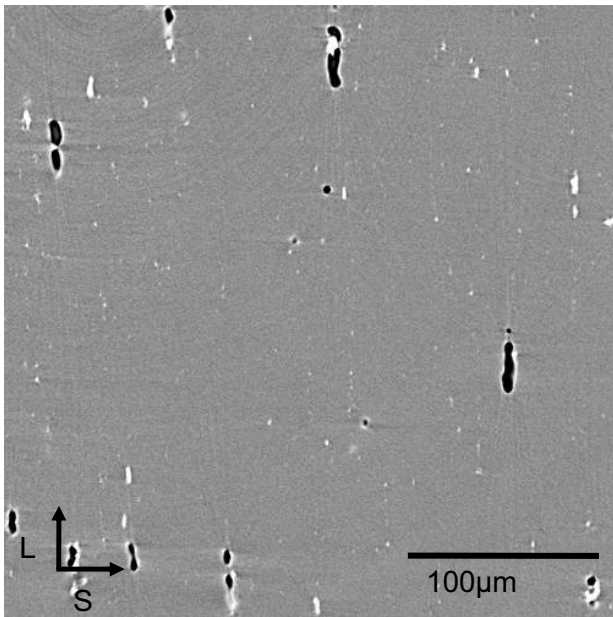
(b)
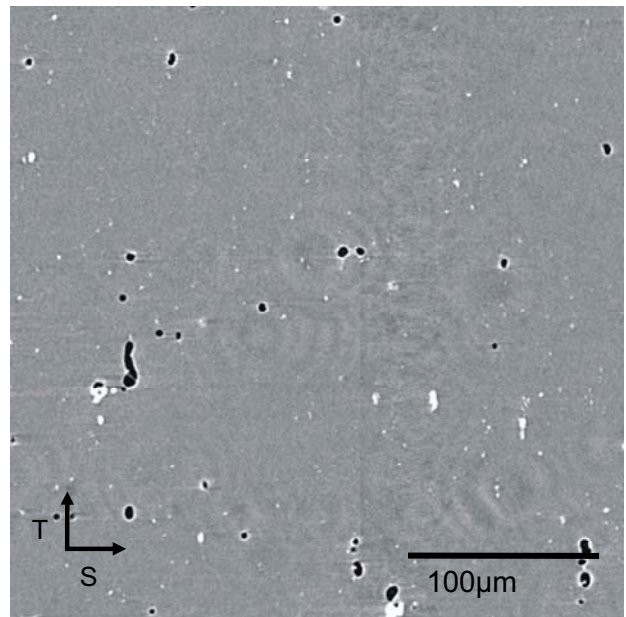
Figure 5: (a) 2D image of the as received material in the L-S plane (b) 2D image of the as received material in the T-S plane

Figure 6

(a)

(b)

(c)
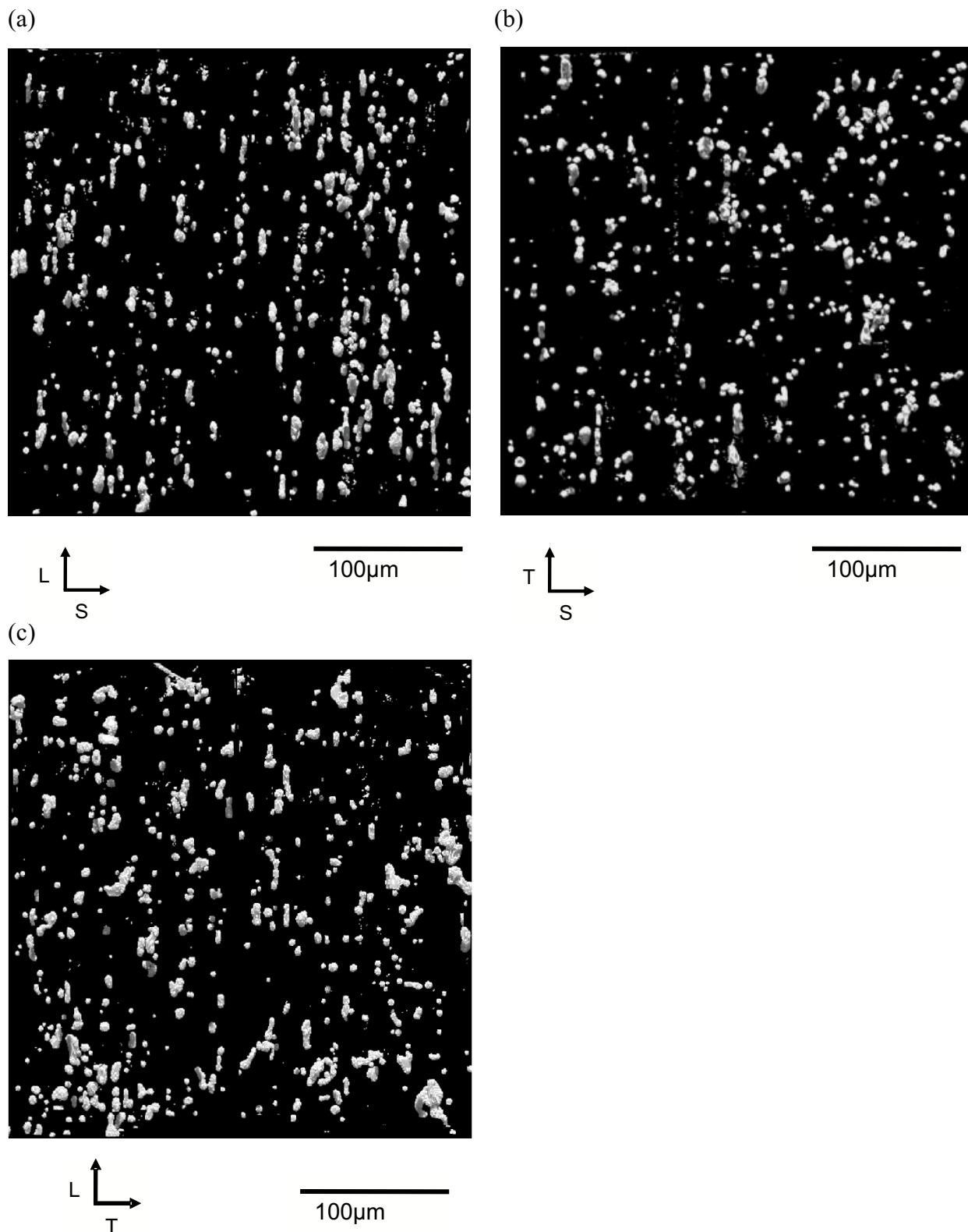
Figure 6: 3D rendering of pores in a volume of 350μm x 350μm x 180μm of the as received material in: (a) the L-S plane, (b) the T-S plane and (c) the L-T plane. (As a projection of voids in a volume of material is shown, the void content appears significantly higher than the actual volume fraction).
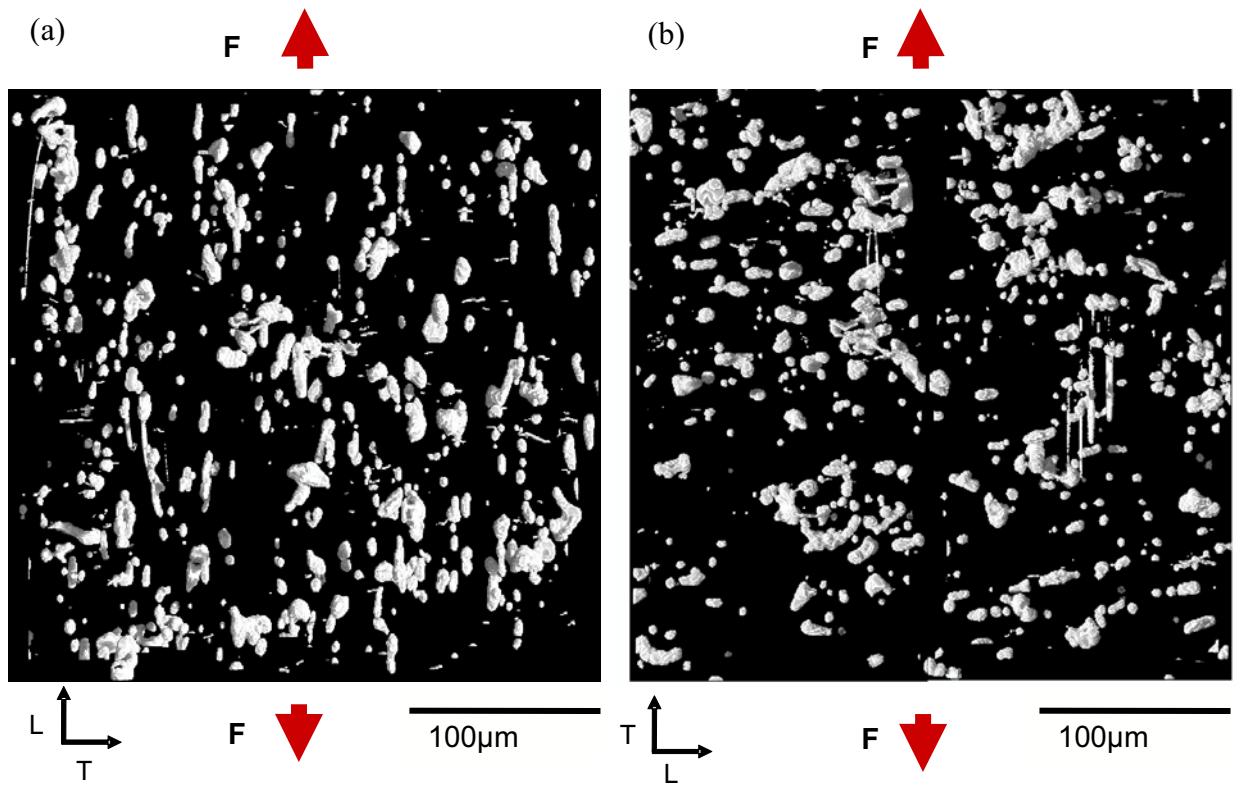
Figure 7
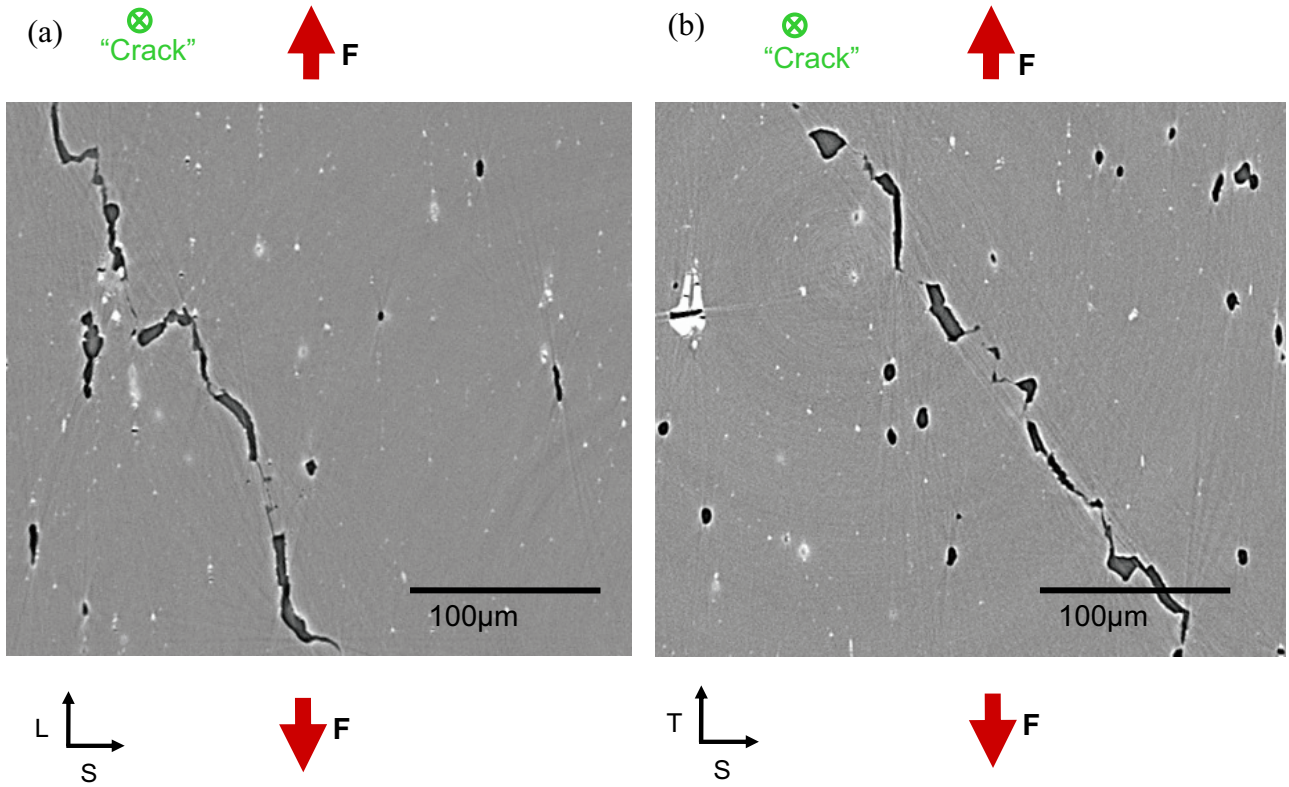
Figure 7: 2D SRCT sections normal to the crack growth: (a) L-T test orientation and (b) T-L test orientation.

Figure

8
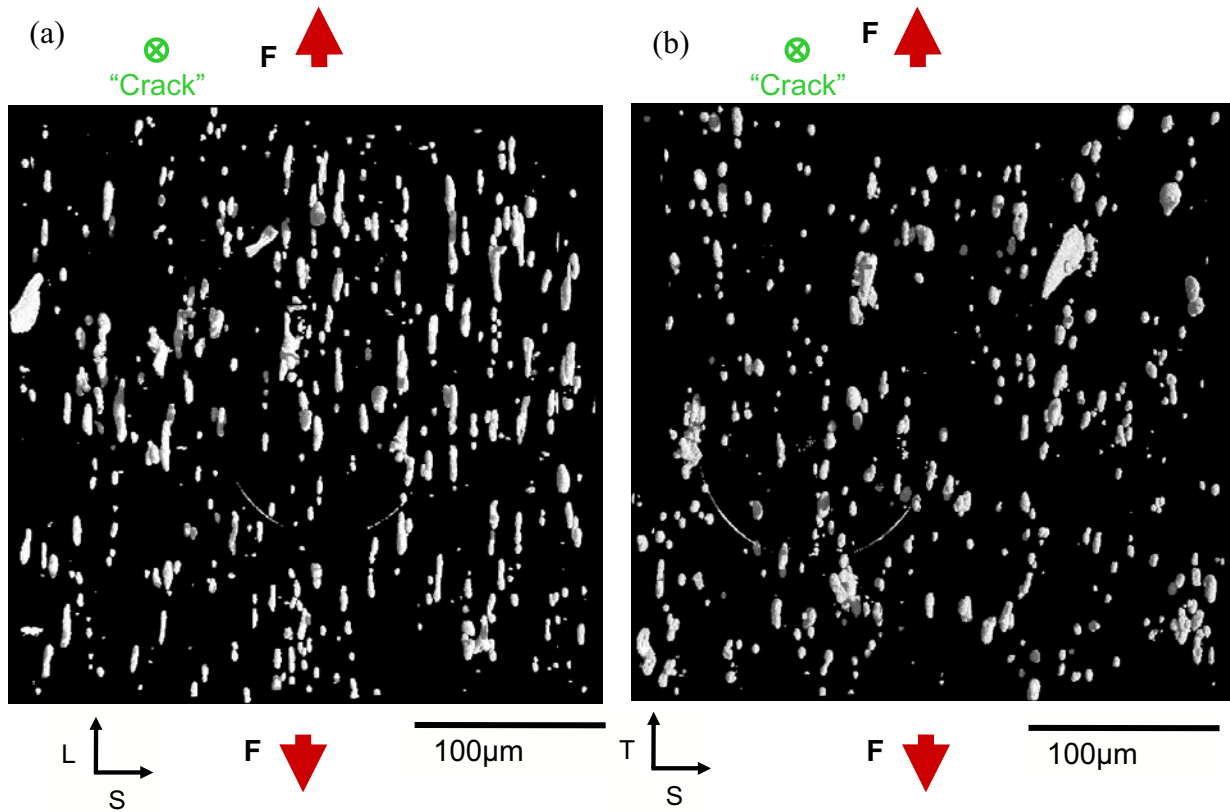
Figure 8: 3D void distribution and morphology : (a) in the L-S plane for L-T loading, and (b) in the T-S plane for T-L loading. (As a projection of voids in a volume of material is shown, the void content appears significantly higher than the actual volume fraction).

Figure 9

Figure 9: 3D void distribution and morphology in a volume of 350μm x 350μm x 180μm in the L-T plane for: (a) L-T loading, and (b) T-L loading. (As a projection of voids in a volume of material is shown, the void content appears significantly higher than the actual volume fraction).
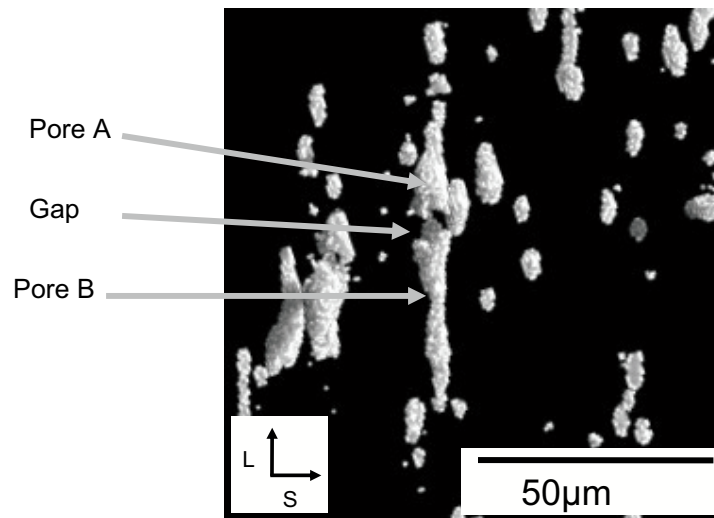
Figure 10

Figure 10: 3D Close-up image of a coalescing elongated voids in the L-T sample in one column
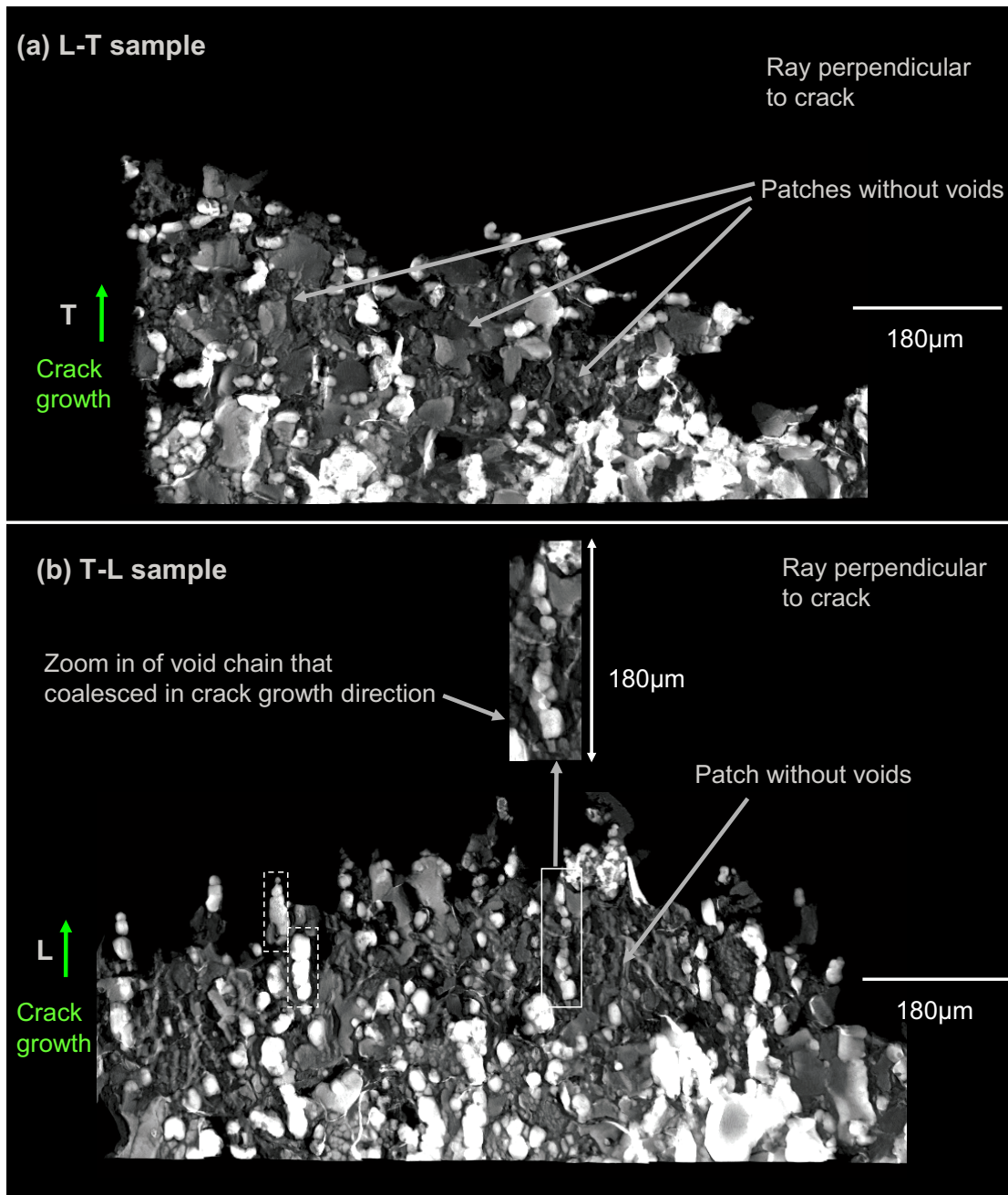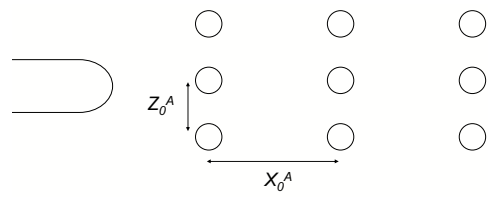
Figure 11

Figure 11: Representation of the crack tip via the "sum along ray" algorithm for: (a) L-T loading, and (b) T-L loading. Two coalescing void chains at the crack tip are highlighted by dashed boxes.
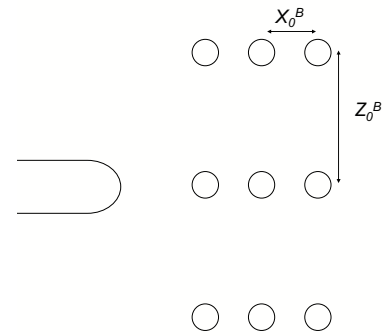
Figure 12

(a)

(b)

Figure 12: Two different crack plane orientations in a material exhibiting initially anisotropic

spacing (after [10])